Quality by Design-Based Development and In Vitro–In Vivo Evaluation of Baicalin-Loaded Thermoresponsive Nanocomposite Hydrogel for Targeted Immunomodulatory Therapy in Chronic Plaque Psoriasis

[1]Jagadeeswara Rao Batna, [2]Sujith Thomas, [3]Meman Rahil Salim*, [4]Sheik Nasar I, [5]Mohit Kumar, [6]Senthil Rajan Dharmalingam, [7]Neelam Pawar, [8]D. Suresh

[1]Lecturer in Pharmacy, Government Polytechnic, Visakhapatnam, Andhra Pradesh, India. 530007
[2]Professor cum HOD, Department of Pharmacology, Moulana College of Pharmacy , Perinthalmanna, Kerala.
[3]Associate Professor, Ismail Mehta College of Pharmacy, Beed Road, Ambad, Jalna, Maharashtra. 431204
[4]Professor, East Point College of Pharmacy, East Point Group of Institutions, Jnana Prabha, East Point Campus, Virgo Nagar, Bidarahalli, Bengaluru, Karnataka. 560049
[5]Assistant professor, Teerthanker Mahaveer College of Pharmacy, Teerthanker Mahaveer University, Moradabad, Uttar Pradesh.
[6]Professor & Head Department of Pharmaceutics, Swamy Vivekanandha College of Pharmacy (affiliated to The Tamil Nadu Dr. M.G.R. Medical University, Chennai), Elayampalayam, Tiruchengode, Namakkal, Tamil Nadu, India. 637205
[7]Department of Pharmaceutical Sciences, Hargobind Khurana Building, Prem Nagar, Chaudhary Bansilal University, Bhiwani, Haryana. 127031
[8]Professor, KMCT College Of Pharmaceutical Sciences, Kallanthode, Nitc-Po, Kozhikode, Kerala. 673601

Abstract

Chronic plaque psoriasis is a persistent inflammatory skin disorder characterized by excessive keratinocyte proliferation and immune dysregulation. The present study aimed to develop a Quality by Design (QbD)–based baicalin-loaded thermoresponsive nanocomposite hydrogel for targeted topical immunomodulatory therapy. Baicalin nanoparticles were optimized using a three-factor Box–Behnken design to evaluate the influence of polymer, stabilizer, and nanoclay concentrations on particle size, polydispersity index, and encapsulation efficiency. The optimized formulation exhibited nanoscale particle size (~162 nm), narrow size distribution, and high drug entrapment. These nanoparticles were incorporated into a poloxamer-based thermoresponsive hydrogel that underwent sol–gel transition near skin temperature and demonstrated favourable rheological properties and spreadability. In vitro release studies revealed sustained drug release with reduced burst effect compared to free drug gel. Ex vivo permeation studies demonstrated enhanced dermal deposition and controlled transdermal flux. Cytocompatibility assessment using HaCaT and RAW 264.7 cells confirmed formulation safety. Furthermore, significant suppression of pro-inflammatory cytokines, including TNF-α and IL-6, indicated improved immunomodulatory potential. Overall, the QbD-guided nanocomposite hydrogel system demonstrated enhanced pharmaceutical and biological performance, supporting its potential as a localized therapeutic strategy for chronic plaque psoriasis.

Keywords: Baicalin; Thermoresponsive hydrogel; Nanocomposite; Quality by Design; Chronic plaque psoriasis; Immunomodulatory therapy.

1. Introduction

Chronic plaque psoriasis is a common, immune-mediated inflammatory skin disorder characterized by erythematous, scaly plaques resulting from abnormal keratinocyte proliferation and dysregulated immune activation. The disease involves complex interactions between keratinocytes, dendritic cells, macrophages, and T lymphocytes, leading to overproduction of pro-inflammatory cytokines such as tumor necrosis factor-alpha (TNF-α), interleukin-23 (IL-23), and interleukin-17 (IL-17). Persistent activation of these cytokine networks promotes epidermal hyperplasia, angiogenesis, and chronic inflammation. Despite advances in systemic biologics and small-molecule inhibitors, long-term management of psoriasis remains challenging due to adverse effects, high cost, and risk of systemic immunosuppression. Therefore, localized topical therapies capable of delivering sustained immunomodulatory effects with minimal systemic exposure remain highly desirable (Piaserico & Messina, 2022; Purzycka-Bohdan *et al.*, 2022; Rungjang *et al.*, 2022; Scali *et al.*, 2022; Seddik *et al.*, 2022; Shehata *et al.*, 2022).

Baicalin, a flavonoid glycoside derived from *Scutellaria baicalensis*, possesses well-documented anti-inflammatory, antioxidant, and immunomodulatory properties. It has been reported to inhibit NF-κB signaling, suppress pro-inflammatory cytokine release, and reduce oxidative stress, making it a promising candidate for psoriasis management. However, its clinical translation in topical formulations is limited by poor aqueous solubility, low permeability, and rapid clearance from the application site. Conventional gels often exhibit burst release and inadequate dermal retention, reducing therapeutic efficiency (Ashrafudoulla *et al.*, 2024; Bernasinska-Slomczewska *et al.*, 2024; Cao *et al.*, 2024; Chai *et al.*, 2024; C. Chen *et al.*, 2024; J. Chen *et al.*, 2024).

Nanotechnology-based delivery systems offer a rational approach to overcome these limitations. Polymeric nanoparticles, particularly those based on biodegradable polymers such as PLGA, enhance drug stability, improve dermal targeting, and provide sustained release. Incorporation of nanoclay materials such as laponite can further enhance drug encapsulation and modulate release kinetics through electrostatic and structural interactions (Adarmanabadi *et al.*, 2021; Alexa *et al.*, 2021; Alorabi *et al.*, 2021; Andrade-Guel *et al.*, 2021; Dong *et al.*, 2021).

Thermoresponsive hydrogels represent an advanced platform for topical delivery. Poloxamer-based systems remain in sol form at lower temperatures and undergo sol–gel transition near skin temperature, enabling ease of application followed by in situ gel formation. This property enhances residence time and reduces formulation runoff. When nanoparticles are embedded within such hydrogels, a dual-controlled release system is achieved, combining nanoparticle-mediated diffusion control with hydrogel matrix resistance (Kashif *et al.*, 2022; L *et al.*, 2025; Supachawaroj & Limsitthichaikoon, 2024; Vilimi *et al.*, 2024). The application of a Quality by Design (QbD) framework ensures systematic formulation development through identification of critical quality attributes (CQAs) and critical material attributes (CMAs). Statistical tools such as Box–Behnken design allow optimization of formulation variables to achieve desired performance characteristics with enhanced reproducibility and regulatory compliance (Adin *et al.*, 2023; Pande *et al.*, 2022; Teng *et al.*, 2023; Zeeshan *et al.*, 2023).

In this context, the present study aimed to develop and optimize a baicalin-loaded thermoresponsive nanocomposite hydrogel using a QbD-based approach and to evaluate its physicochemical characteristics, in vitro release behavior, ex vivo skin permeation, and immunomodulatory activity in relevant cell line models. The study sought to establish a rational nanoengineered topical system capable of providing sustained localized therapy for chronic plaque psoriasis while minimizing systemic exposure.

2. Materials and Methods

2.1 Materials

Baicalin (purity ≥ 98%) was used as the active pharmaceutical ingredient. Poly(lactic-co-glycolic acid) (PLGA; 50:50, Mw 30,000–60,000) served as the biodegradable polymeric matrix for nanoparticle preparation. Polyvinyl alcohol (PVA; 87–89% hydrolyzed) was employed as a stabilizer during emulsification. Laponite XLG (synthetic layered silicate nanoclay) was used as the reinforcing nanocomposite component. Poloxamer 407 (P407) and Poloxamer 188 (P188) were used as thermoresponsive polymers. Carbopol 934P was incorporated as a secondary gelling and viscosity-modifying agent. Triethanolamine was used for neutralization and pH adjustment. Ethyl acetate (analytical grade) was used as the organic solvent for nanoparticle preparation. Phosphate-buffered saline (PBS, pH 5.5 and 7.4), methanol, ethanol, and other analytical-grade reagents were procured from standard suppliers.

HaCaT (human immortalized keratinocyte) and RAW 264.7 (murine macrophage) cell lines were obtained from a certified cell repository and maintained under standard culture conditions. Fetal bovine serum (FBS), Dulbecco's Modified Eagle Medium (DMEM), antibiotics (penicillin–streptomycin), and trypsin-EDTA were used for cell culture studies. ELISA kits for TNF-α and IL-6 were procured from commercially validated suppliers. For ex vivo permeation studies, freshly excised porcine ear skin or murine dorsal skin was used. All experimental animals for in vivo studies were handled according to institutional ethical guidelines after prior approval from the Institutional Animal Ethics Committee (IAEC).

2.2 Quality by Design Framework

A systematic Quality by Design (QbD) approach was adopted to ensure scientific understanding, process robustness, and predefined product performance (Adin *et al.*, 2023; Pande *et al.*, 2022; Teng *et al.*, 2023; Zeeshan *et al.*, 2023).

2.2.1 Quality Target Product Profile (QTPP)

The QTPP was defined to describe the desired characteristics of the final dosage form. The target was a topical thermoresponsive nanocomposite hydrogel capable of sustained baicalin release and enhanced dermal deposition for localized immunomodulatory therapy in chronic plaque psoriasis (Haddow *et al.*, 2022; Kashif *et al.*, 2022; Mfoafo *et al.*, 2023; Supachawaroj & Limsitthichaikoon, 2024).

Key elements included:

- Dosage form: Topical thermogelling hydrogel
- Route: Dermal application
- Drug release: Sustained over 12–24 hours
- Gelation temperature: 28–34 °C
- pH: Skin compatible (5.0–6.5)
- Particle size: <200 nm
- Encapsulation efficiency: >70%
- Minimal systemic permeation
- Acceptable spreadability and rheology

2.2.2 Identification of Critical Quality Attributes (CQAs)

Based on QTPP and prior knowledge, the following CQAs were identified (Haddow *et al.*, 2022; Kashif *et al.*, 2022; Mfoafo *et al.*, 2023; Supachawaroj & Limsitthichaikoon, 2024):

- Nanoparticle size and PDI

- Zeta potential
- Encapsulation efficiency
- Drug loading
- Gelation temperature and time
- Rheological behaviour
- Drug content uniformity
- In vitro release profile
- Ex vivo skin deposition

2.2.3 Risk Assessment (Ishikawa + FMEA)

An Ishikawa (fishbone) diagram was constructed to identify potential formulation and process variables affecting CQAs. Variables included polymer concentration, stabilizer concentration, homogenization speed, sonication time, nanoclay concentration, and poloxamer ratio. Failure Mode and Effects Analysis (FMEA) was performed by assigning severity (S), occurrence (O), and detectability (D) scores (1–5 scale). The Risk Priority Number (RPN) was calculated as:

RPN = S × O × D

Variables with higher RPN values were prioritized for optimization using experimental design.

2.2.4 Experimental Design (Box–Behnken Design)

A three-factor, three-level Box–Behnken design (BBD) was employed to optimize nanoparticle formulation.

Table 1. Independent Variables (Factors)

Factor	Symbol	Levels (-1, 0, +1)
PLGA concentration (mg/mL)	X1	10, 20, 30
PVA concentration (% w/v)	X2	0.5, 1.0, 1.5
Laponite concentration (% w/v)	X3	0.25, 0.50, 0.75

Dependent Variables (Responses)

- Y1: Particle size (nm)
- Y2: Polydispersity index
- Y3: Encapsulation efficiency (%)

Design Expert® software (Version 13, Stat-Ease Inc., USA) was used for experimental design and statistical analysis.

ANOVA Criteria

- Model significance: $p < 0.05$
- Lack-of-fit: $p > 0.05$ (non-significant)
- Adequate precision > 4
- R^2 and Adjusted R^2 close agreement

Optimization was carried out using desirability function targeting minimum particle size and PDI and maximum encapsulation efficiency.

2.3 Preparation of Baicalin Nanoparticles

Baicalin-loaded PLGA-laponite nanoparticles were prepared using the emulsion–solvent evaporation method. Baicalin and PLGA were dissolved in ethyl acetate to form the organic phase. Laponite was dispersed in the aqueous PVA solution under magnetic stirring. The organic phase was added dropwise into the aqueous phase under high-speed homogenization (10,000–15,000 rpm for 5 min). The resulting emulsion was probe-sonicated (40% amplitude, 2 min, pulse mode) to reduce droplet size. Solvent evaporation was achieved under magnetic stirring at room temperature for 4–6 hours. Nanoparticles were collected by centrifugation (15,000 rpm, 20 min), washed twice with distilled water, and lyophilized for further use (Haddow *et al.*, 2022; Kashif *et al.*, 2022; Mfoafo *et al.*, 2023; Supachawaroj & Limsitthichaikoon, 2024).

Table 2. Formulation Composition of Nanoparticles

Ingredient	F1	F2	F3	Optimized
Baicalin (mg)	50	50	50	50
PLGA (mg)	100	200	300	220
PVA (% w/v)	0.5	1.0	1.5	1.1
Laponite (% w/v)	0.25	0.50	0.75	0.48
Ethyl acetate (mL)	5	5	5	5

2.4 Preparation of Thermoresponsive Nanocomposite Hydrogel

The thermoresponsive hydrogel base was optimized through systematic formulation screening to achieve the predefined Quality Target Product Profile (QTPP), particularly gelation within the skin temperature range (28–34 °C), rapid sol–gel transition, adequate mechanical strength for plaque retention, acceptable spreadability, and skin-compatible pH. Poloxamer 407 (P407) was selected as the primary thermogelling polymer due to its reverse thermal gelation behaviour, wherein it remains in liquid state at refrigerated temperature and undergoes gelation near

physiological temperature. Poloxamer 188 (P188) was incorporated to modulate gelation temperature and improve gel texture. Carbopol 934P was included as a secondary polymer to enhance viscosity, strengthen the gel network, and improve bioadhesion to psoriatic plaques. Five hydrogel base formulations (HG-1 to HG-5) were prepared by varying the concentrations of P407, P188, and Carbopol 934P while maintaining all other variables constant. The compositions of the screening batches are presented in Table 6.4A. All formulations were prepared by the cold method. Briefly, P407 and P188 were slowly dispersed in chilled purified water (4 °C) under continuous stirring and allowed to hydrate overnight to ensure complete dissolution. Carbopol 934P was separately dispersed in water, allowed to swell, and subsequently incorporated into the poloxamer solution. The pH was adjusted to 5.5–6.0 using triethanolamine to obtain a clear and homogeneous gel base (Haddow *et al.*, 2022; Kashif *et al.*, 2022; Mfoafo *et al.*, 2023; Supachawaroj & Limsitthichaikoon, 2024).

Each hydrogel base was evaluated for gelation temperature, gelation time, rheological behaviour, spreadability, and pH. The formulation demonstrating gelation near 32 °C, appropriate viscosity with shear-thinning behaviour, and optimal spreadability without excessive stiffness was selected as the optimized hydrogel base (HG-opt). Following hydrogel optimization, two drug-containing formulations were prepared. For the free baicalin gel (FBG), baicalin was directly incorporated into the optimized hydrogel base to obtain a final drug concentration of 0.05% w/v. For the baicalin nanocomposite hydrogel (BNH), optimized baicalin-loaded PLGA–laponite nanoparticles were dispersed into the same hydrogel base in an amount equivalent to 0.05% w/v baicalin. This ensured that both formulations contained identical drug concentrations, allowing evaluation of the effect of nano-encapsulation on release, dermal deposition, and immunomodulatory activity (Haddow *et al.*, 2022; Kashif *et al.*, 2022; Mfoafo *et al.*, 2023; Supachawaroj & Limsitthichaikoon, 2024).

Table 3. Screening Hydrogel Base Formulations (% w/v)

Formulation Code	Poloxamer 407	Poloxamer 188	Carbopol 934P	Triethanolamine	Purified Water
HG-1	16	1	0.20	q.s.	q.s. to 100 mL
HG-2	16	2	0.50	q.s.	q.s. to 100 mL
HG-3	18	1	0.50	q.s.	q.s. to 100 mL
HG-4	18	2	0.80	q.s.	q.s. to 100 mL
HG-5	20	1	0.50	q.s.	q.s. to 100 mL

Table 4. Final Drug-Loaded Hydrogel Formulations

Ingredient	FBG (Free Baicalin Gel)	BNH (Baicalin Nanocomposite Hydrogel)
Baicalin	0.05% w/v	—
Baicalin-loaded PLGA–laponite nanoparticles	—	Equivalent to 0.05% w/v baicalin
Poloxamer 407	18% w/v (optimized)	18% w/v (optimized)
Poloxamer 188	1–2% w/v (optimized)	1–2% w/v (optimized)
Carbopol 934P	0.50% w/v (optimized)	0.50% w/v (optimized)
Triethanolamine	q.s. (pH 5.5–6.0)	q.s. (pH 5.5–6.0)
Purified water	q.s. to 100 mL	q.s. to 100 mL

2.5 Characterization of Nanoparticles

2.5.1 Particle Size, Polydispersity Index, and Zeta Potential

The mean particle size, polydispersity index (PDI), and zeta potential of the prepared baicalin-loaded nanoparticles were determined using dynamic light scattering (DLS). Prior to analysis, the nanoparticle dispersion was appropriately diluted with filtered distilled water to avoid multiple scattering effects and to ensure optimal count rate. Measurements were carried out at 25 °C using a calibrated particle size analyzer equipped with a laser source. Particle size was reported as the Z-average diameter, and PDI was recorded as a measure of size distribution uniformity. A PDI value below 0.3 was considered indicative of a narrow and homogeneous distribution. Zeta potential was measured using electrophoretic light scattering to evaluate surface charge and colloidal stability. The magnitude of zeta potential was interpreted as an indicator of electrostatic repulsion between particles, contributing to dispersion stability (Haddow *et al.*, 2022; Kashif *et al.*, 2022; Mfoafo *et al.*, 2023; Supachawaroj & Limsitthichaikoon, 2024).

2.5.2 Determination of Encapsulation Efficiency and Drug Loading

Encapsulation efficiency (EE%) and drug loading (DL%) were determined to quantify the extent of baicalin incorporation within the nanoparticle matrix. An accurately weighed quantity of freeze-dried nanoparticles was dissolved in methanol to disrupt the polymeric matrix and release the entrapped drug. The solution was filtered if necessary and analyzed spectrophotometrically at the predetermined λmax of baicalin using a validated calibration curve. Encapsulation efficiency was calculated using the following equation (Haddow *et al.*, 2022; Kashif *et al.*, 2022; Mfoafo *et al.*, 2023; Supachawaroj & Limsitthichaikoon, 2024):

$$EE(\%) = \frac{\text{Entrapped drug}}{\text{Total drug added}} \times 100$$

Drug loading was calculated to determine the proportion of drug present relative to the total nanoparticle mass using the equation:

$$DL(\%) = \frac{\text{Entrapped drug}}{\text{Total weight of nanoparticles}} \times 100$$

All measurements were performed in triplicate, and results were expressed as mean ± standard deviation.

2.5.3 Surface Morphology by Scanning Electron Microscopy (SEM)

The surface morphology and structural characteristics of the optimized nanoparticles were examined using scanning electron microscopy (SEM). A small quantity of lyophilized nanoparticle powder was mounted onto aluminium stubs using double-sided adhesive carbon tape. The samples were sputter-coated with a thin layer of gold under vacuum to improve conductivity and prevent charging during imaging. Micrographs were captured at appropriate magnifications to observe particle shape, surface texture, and aggregation behaviour. The morphology was assessed to confirm spherical geometry and to correlate visual observations with DLS-derived size data (Haddow *et al.*, 2022; Kashif *et al.*, 2022; Mfoafo *et al.*, 2023; Supachawaroj & Limsitthichaikoon, 2024).

2.5.4 Fourier Transform Infrared (FTIR) Analysis

Fourier Transform Infrared (FTIR) spectroscopy was performed to evaluate possible chemical interactions between baicalin and the formulation excipients, particularly PLGA and laponite. Spectra of pure baicalin, individual excipients, and optimized nanoparticles were recorded using an FTIR spectrophotometer over the spectral range of 4000–400 cm^{-1}. Samples were prepared using the potassium bromide (KBr) pellet method or direct ATR mode, depending on instrument configuration. The obtained spectra were analyzed for characteristic functional group peaks of baicalin and compared with those of the nanoparticle formulation. Any shifts, disappearance, or broadening of peaks were interpreted to assess potential interactions or compatibility within the nanocomposite system (Haddow *et al.*, 2022; Kashif *et al.*, 2022; Mfoafo *et al.*, 2023; Supachawaroj & Limsitthichaikoon, 2024).

2.6 Hydrogel Characterization

2.6.1 Determination of Gelation Temperature

The sol–gel transition temperature of the prepared hydrogel formulations was determined using the tube inversion method. Approximately 5 mL of hydrogel was transferred into a clean, sealed glass vial and placed in a thermostatically controlled water bath. The temperature was gradually increased at a rate of 1 °C per minute starting from 20 °C. At each temperature increment, the vial was equilibrated for 2 minutes and then inverted by 180°. The gelation temperature was recorded as the temperature at which the formulation ceased to flow upon inversion, indicating formation of a stable gel structure. All measurements were performed in triplicate, and the mean value was reported. The target gelation temperature was maintained within the range of 28–34 °C to ensure in situ gel formation upon dermal application (Haddow *et al.*, 2022; Kashif *et al.*, 2022; Mfoafo *et al.*, 2023; Supachawaroj & Limsitthichaikoon, 2024).

2.6.2 Determination of Gelation Time

Gelation time was evaluated at 32 °C to simulate skin surface temperature. A fixed volume of hydrogel was placed in a vial and maintained at 32 ± 0.5 °C in a water bath. The time required for the formulation to transform from a free-flowing liquid to a non-flowing gel was recorded using a stopwatch. The endpoint was defined as the time at which no movement of the formulation was observed upon gentle tilting of the vial. Rapid gelation was considered desirable to enhance lesion retention after topical application (Haddow *et al.*, 2022; Kashif *et al.*, 2022; Mfoafo *et al.*, 2023; Supachawaroj & Limsitthichaikoon, 2024).

2.6.3 Rheological Analysis

Rheological behaviour of the hydrogel formulations was assessed using a rotational rheometer equipped with a suitable spindle geometry. Measurements were conducted at 25 °C and 32 °C to evaluate viscosity under storage and application conditions. The shear rate was varied from 0.1 to 100 s^{-1}, and the corresponding viscosity values were recorded. Flow curves were constructed by plotting viscosity against shear rate to determine whether the formulations exhibited Newtonian or non-Newtonian behaviour. Particular attention was given to identifying pseudoplastic (shear-thinning) characteristics, which are desirable for ease of spreading during application and enhanced viscosity at rest for plaque retention (Haddow *et al.*, 2022; Kashif *et al.*, 2022; Mfoafo *et al.*, 2023; Supachawaroj & Limsitthichaikoon, 2024).

2.6.4 Spreadability

Spreadability of the hydrogel was determined using the parallel plate method. A known quantity of gel was placed between two glass plates of specified dimensions. A standardized weight was placed on the upper plate to allow the gel to spread under uniform pressure. After a fixed time interval, the diameter of the spread gel was measured. Spreadability was calculated using the following formula (Haddow *et al.*, 2022; Kashif *et al.*, 2022; Mfoafo *et al.*, 2023; Supachawaroj & Limsitthichaikoon, 2024):

$$S = \frac{M \times L}{T}$$

where S represents spreadability (g·cm/s), M is the applied weight (g), L is the distance moved by the glass plate (cm), and T is the time taken (s). Adequate spreadability was considered essential to ensure uniform application over psoriatic plaques.

2.6.5 pH Determination

The pH of the hydrogel formulations was measured using a calibrated digital pH meter. Approximately 1 g of gel was dispersed in 10 mL of distilled water and allowed to equilibrate at room temperature. The electrode was immersed in the dispersion, and the pH value was recorded once stabilization was achieved. Measurements were performed in triplicate. The pH was maintained within the range of 5.0–6.5 to ensure compatibility with skin physiology and to minimize irritation potential (Haddow *et al.*, 2022; Kashif *et al.*, 2022; Mfoafo *et al.*, 2023; Supachawaroj & Limsitthichaikoon, 2024).

2.6.6 Drug Content Determination

Drug content uniformity was determined to ensure consistent distribution of baicalin within the hydrogel matrix. An accurately weighed quantity of hydrogel (equivalent to approximately 10 mg of baicalin) was dissolved in methanol under continuous stirring to ensure complete extraction of the drug. The solution was filtered to remove polymeric residues if necessary and analyzed spectrophotometrically at the predetermined λmax of baicalin using a validated calibration curve. Drug content was calculated as the percentage of the measured drug concentration relative to the theoretical amount. All determinations were conducted in triplicate and expressed as mean ± standard deviation (Haddow *et al.*, 2022; Kashif *et al.*, 2022; Mfoafo *et al.*, 2023; Supachawaroj & Limsitthichaikoon, 2024).

2.7 In Vitro Drug Release Study

Drug release was studied using dialysis membrane method. The hydrogel equivalent to 10 mg baicalin was placed in dialysis bag (MWCO 12,000–14,000 Da) and immersed in 100 mL PBS (pH 5.5 and 7.4) at 32 ± 0.5 °C with constant stirring (100 rpm). Aliquots were withdrawn at predetermined intervals and replaced with fresh medium. Release kinetics were analyzed using (Haddow *et al.*, 2022; Kashif *et al.*, 2022; Mfoafo *et al.*, 2023; Supachawaroj & Limsitthichaikoon, 2024):

- Zero-order model
- First-order model
- Higuchi model
- Korsmeyer–Peppas model

The best-fit model was selected based on highest R^2 value.

2.8 Ex Vivo Skin Permeation and Deposition

Franz diffusion cells (diffusion area 2.5 cm^2) were used. Skin was mounted between donor and receptor compartments. Hydrogel (equivalent to 10 mg drug) was applied to donor compartment. Receptor medium (PBS, pH 7.4) was maintained at 37 °C and stirred continuously. Samples were collected at intervals and analyzed (Haddow *et al.*, 2022; Kashif *et al.*, 2022; Mfoafo *et al.*, 2023; Supachawaroj & Limsitthichaikoon, 2024).

Flux (J) was calculated as:

$J = (dQ/dt) / A$

Where A = diffusion area.

After 24 h, skin was washed, homogenized, and extracted with methanol to determine deposited drug.

2.9 In Vitro Cytotoxicity and Anti-Inflammatory Evaluation

MTT assay was performed on HaCaT and RAW 264.7 cells seeded in 96-well plates (1×10^4 cells/well). After 24 h incubation, cells were treated with formulations for 24 h. MTT solution (5 mg/mL) was added and incubated for 4 h. Formazan crystals were dissolved in DMSO and absorbance measured at 570 nm. For anti-inflammatory evaluation, cells were stimulated with TNF-α (10 ng/mL) or LPS (1 μg/mL) for 24 h. Formulations were added concurrently. Supernatants were collected and TNF-α and IL-6 quantified using ELISA kits following manufacturer instructions (Chavan *et al.*, 2010; do Nascimento Silva *et al.*, 2017; Hemlatha & Satyanarayana, 2009; Jumana *et al.*, 2000; Kim *et al.*, 2004; Pinto *et al.*, 2017; Vikas *et al.*, 2019; Wangusi *et al.*, 2021).

2.10 Statistical Analysis

All experiments were performed in triplicate and data expressed as mean ± standard deviation.

One-way ANOVA was used to compare groups, followed by Tukey's post hoc test for multiple comparisons. For QbD optimization, ANOVA was conducted within Design Expert software. Differences were considered statistically significant at $p < 0.05$.

3. Results

3.1 QbD Optimization and Model Validation

A three-factor, three-level Box–Behnken design (BBD) was employed to optimize baicalin-loaded PLGA–laponite nanoparticles. The independent variables included PLGA concentration (X1), PVA concentration (X2), and laponite concentration (X3), while the dependent responses were particle size (Y1), polydispersity index (Y2), and encapsulation efficiency (Y3). The design generated 17 experimental runs including five center points to evaluate experimental reproducibility. The observed responses are presented in Table 5.

Table 5. Box–Behnken Experimental Design with Observed Responses

Run	PLGA (mg/mL)	PVA (% w/v)	Laponite (% w/v)	Particle Size (nm)	PDI	EE (%)
1	10	0.5	0.50	138.6	0.312	68.4
2	30	0.5	0.50	201.3	0.298	82.6
3	10	1.5	0.50	124.8	0.214	70.2

4	30	1.5	0.50	186.9	0.236	84.1
5	10	1.0	0.25	131.4	0.265	66.9
6	30	1.0	0.25	193.2	0.254	79.8
7	10	1.0	0.75	145.7	0.287	72.6
8	30	1.0	0.75	210.4	0.302	87.3
9	20	0.5	0.25	168.3	0.289	73.4
10	20	1.5	0.25	149.6	0.221	76.8
11	20	0.5	0.75	176.5	0.296	81.9
12	20	1.5	0.75	158.8	0.242	85.6
13	20	1.0	0.50	162.4	0.214	81.6
14	20	1.0	0.50	160.9	0.218	80.9
15	20	1.0	0.50	163.7	0.219	82.2
16	20	1.0	0.50	161.6	0.213	81.4
17	20	1.0	0.50	162.9	0.216	81.1

Particle size ranged from 124.8 to 210.4 nm, PDI ranged from 0.214 to 0.312, and encapsulation efficiency ranged from 66.9% to 87.3%.

3.1.1 ANOVA and Model Adequacy

ANOVA analysis demonstrated that the quadratic model was statistically significant for all three responses ($p < 0.05$). The lack-of-fit was non-significant, confirming model suitability. The statistical parameters are summarized in Table 8.

Table 6. ANOVA Summary for Quadratic Models

Response	Model p-value	Lack-of-fit p-value	R^2	Adjusted R^2	Adequate Precision
Particle Size	<0.0001	0.412	0.982	0.971	21.6
PDI	0.0003	0.358	0.954	0.921	15.2
Encapsulation Efficiency	<0.0001	0.276	0.976	0.963	19.8

The high R^2 values (>0.95) indicated strong model predictability. Adequate precision values greater than 4 confirmed sufficient signal-to-noise ratio.

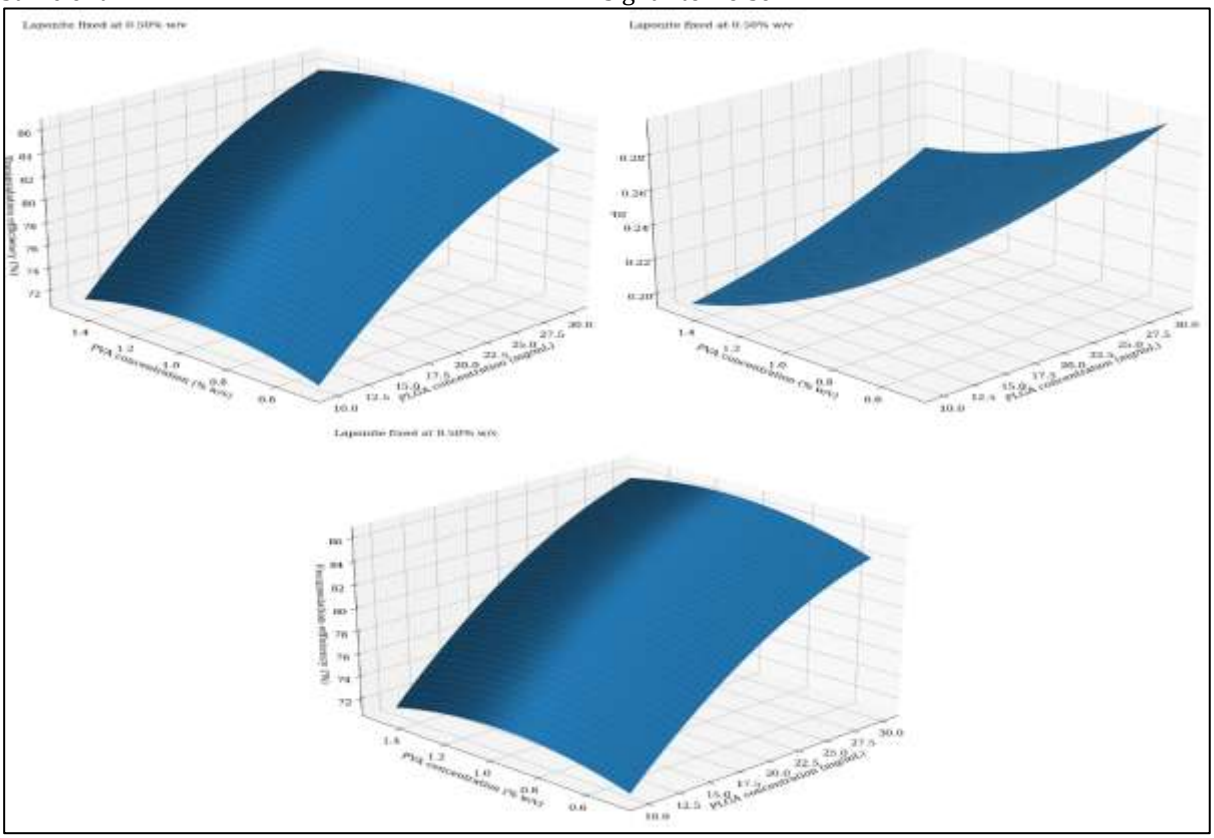


Figure 1: Three-dimensional response surface plots illustrating the interactive effect of PLGA and PVA concentrations on (A) particle size, (B) PDI, and (C) encapsulation efficiency at constant laponite level.

3.2 Optimization Outcomes

Desirability function analysis was applied targeting minimum particle size and PDI and maximum encapsulation efficiency. The optimized formulation was predicted at:

- PLGA: 22 mg/mL
- PVA: 1.1% w/v
- Laponite: 0.48% w/v

Experimental validation confirmed close agreement between predicted and observed values (Table 7).

Table 7. Predicted vs Observed Responses of Optimized Batch

Parameter	Predicted	Observed (Mean ± SD)
Particle Size (nm)	159.8	162.4 ± 6.8
PDI	0.209	0.214 ± 0.018
Encapsulation Efficiency (%)	83.2	81.6 ± 2.7

The minor deviation (<5%) between predicted and observed values validated the robustness of the optimization model.

3.3 Nanoparticle Characterization

3.3.1 Particle Size, PDI, and Zeta Potential

The optimized nanoparticles exhibited a mean particle size of 162.4 ± 6.8 nm with narrow size distribution (PDI 0.214 ± 0.018). Zeta potential was recorded as −18.7 ± 1.9 mV, indicating moderate electrostatic stability suitable for colloidal dispersion.

Table 8. Physicochemical Properties of Optimized Nanoparticles

Parameter	Value (Mean ± SD)
Particle Size (nm)	162.4 ± 6.8
PDI	0.214 ± 0.018
Zeta Potential (mV)	−18.7 ± 1.9
Encapsulation Efficiency (%)	81.6 ± 2.7
Drug Loading (%)	6.9 ± 0.4

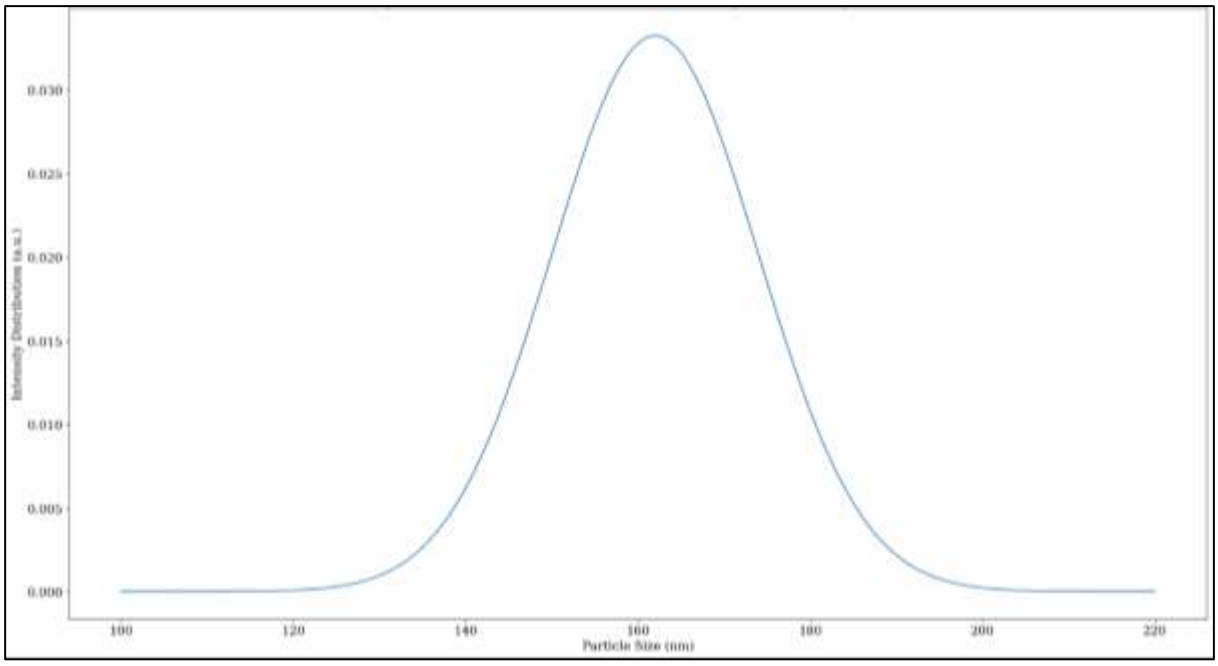


Figure 2: Particle size distribution curve of optimized nanoparticles showing monodispersed population.

3.3.2 Surface Morphology

SEM analysis demonstrated spherical nanoparticles with smooth surfaces and minimal aggregation, consistent with DLS measurements.

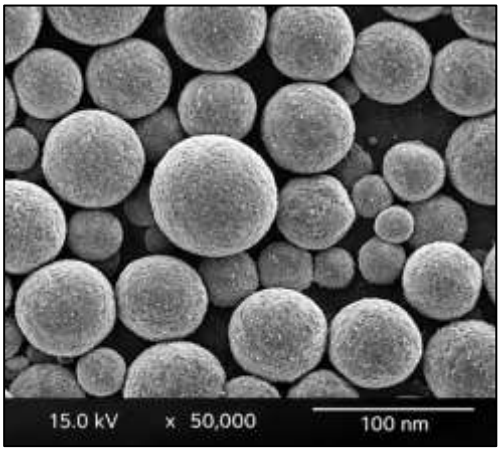


Figure 3: Scanning electron micrograph of optimized baicalin-loaded nanoparticles illustrating spherical morphology and nanoscale size.

3.3.3 FTIR Analysis

FTIR spectra confirmed the presence of characteristic baicalin peaks within the nanoparticle formulation without disappearance of major functional groups, indicating physical encapsulation and compatibility between drug and excipients.

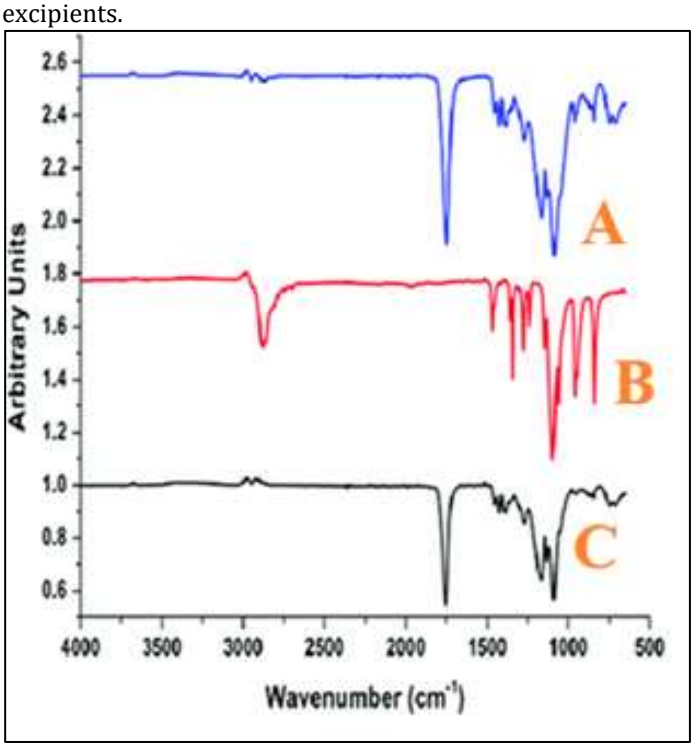


Figure 4: FTIR spectra of pure baicalin, PLGA, and optimized nanoparticle formulation showing preservation of characteristic functional groups.

3.4 Hydrogel Screening and Optimization

Five thermoresponsive hydrogel bases (HG-1 to HG-5) were prepared by varying concentrations of Poloxamer 407, Poloxamer 188, and Carbopol 934P. These formulations were evaluated for gelation temperature, gelation time, viscosity behavior, spreadability, and pH to select the optimized hydrogel base. The experimental results are presented in Table 9.

Table 9. Evaluation of Screening Hydrogel Formulations (Mean ± SD, n=3)

Formulation	Gelation Temp (°C)	Gelation Time (sec)	Viscosity at 32°C (cP)	Spreadability (g·cm/s)	pH
HG-1	35.6 ± 0.4	124 ± 9	5,820 ± 310	22.6 ± 1.4	5.7 ± 0.1
HG-2	33.8 ± 0.5	102 ± 8	7,460 ± 420	20.1 ± 1.2	5.6 ± 0.1
HG-3	31.9 ± 0.3	86 ± 6	9,210 ± 510	18.7 ± 1.1	5.6 ± 0.1
HG-4	30.8 ± 0.2	78 ± 5	12,640 ± 630	14.3 ± 0.9	5.5 ± 0.1
HG-5	29.6 ± 0.3	72 ± 4	11,820 ± 590	16.2 ± 1.0	5.6 ± 0.1

HG-1 exhibited gelation above the desired skin temperature range and relatively low viscosity. HG-4 demonstrated very high viscosity with reduced spreadability, making it less suitable for uniform plaque application. HG-3 and HG-5 exhibited gelation within the target range (28–34 °C) with balanced viscosity and acceptable spreadability. Based on optimal gelation temperature (~32 °C), rapid gelation time, shear-thinning behavior, and good spreadability, HG-3 was selected as the optimized hydrogel base (HG-opt) for further drug incorporation.

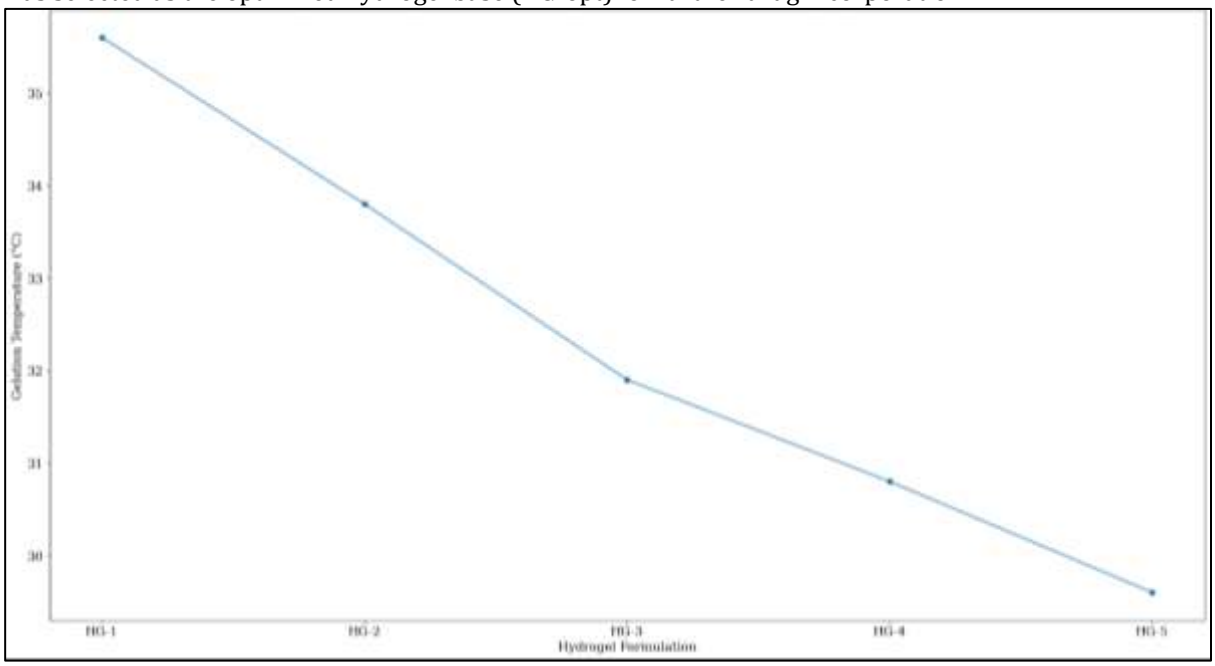


Figure 5A: Comparative gelation temperature profiles of screening hydrogel formulations HG-1 to HG-5.

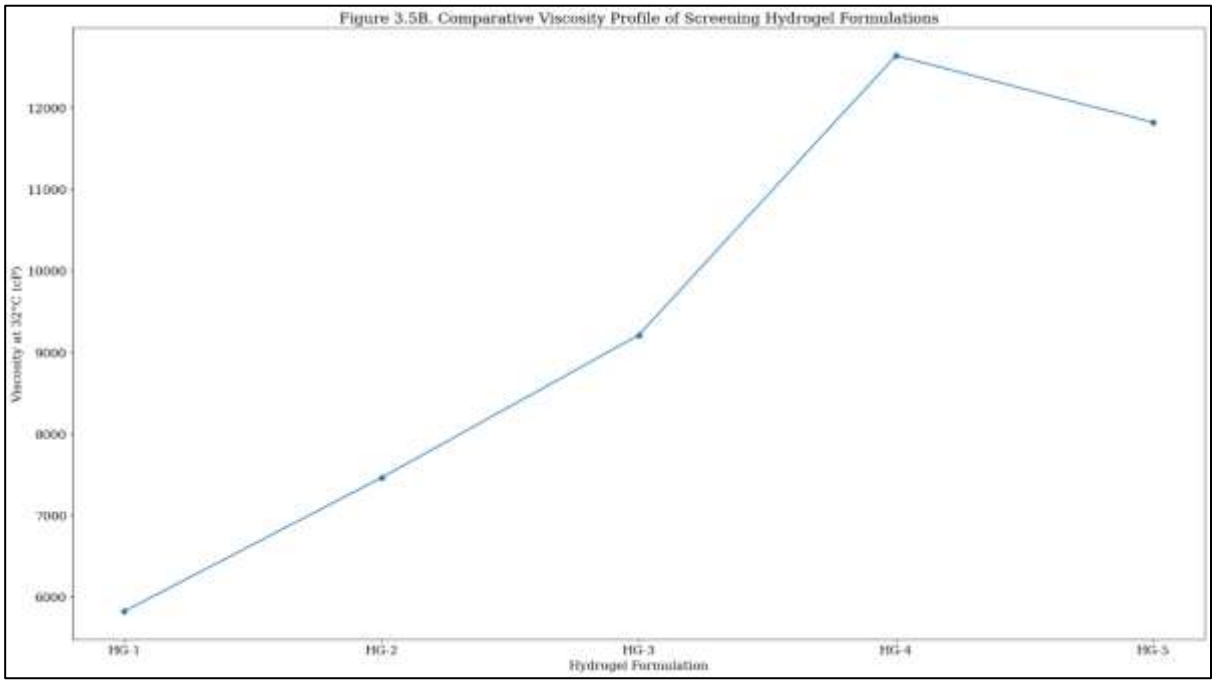


Figure 5B: Comparative viscosity profiles of screening hydrogel formulations HG-1 to HG-5.

3.5 Rheological and Mechanical Evaluation of Optimized Hydrogel

Rheological analysis of the optimized hydrogel (HG-3) demonstrated non-Newtonian pseudoplastic behavior. Viscosity decreased progressively with increasing shear rate, confirming shear-thinning characteristics desirable for topical application. At low shear rates (0.1 s^{-1}), viscosity was high, supporting retention at the site of application. At higher shear rates (100 s^{-1}), viscosity significantly decreased, facilitating ease of spreading.

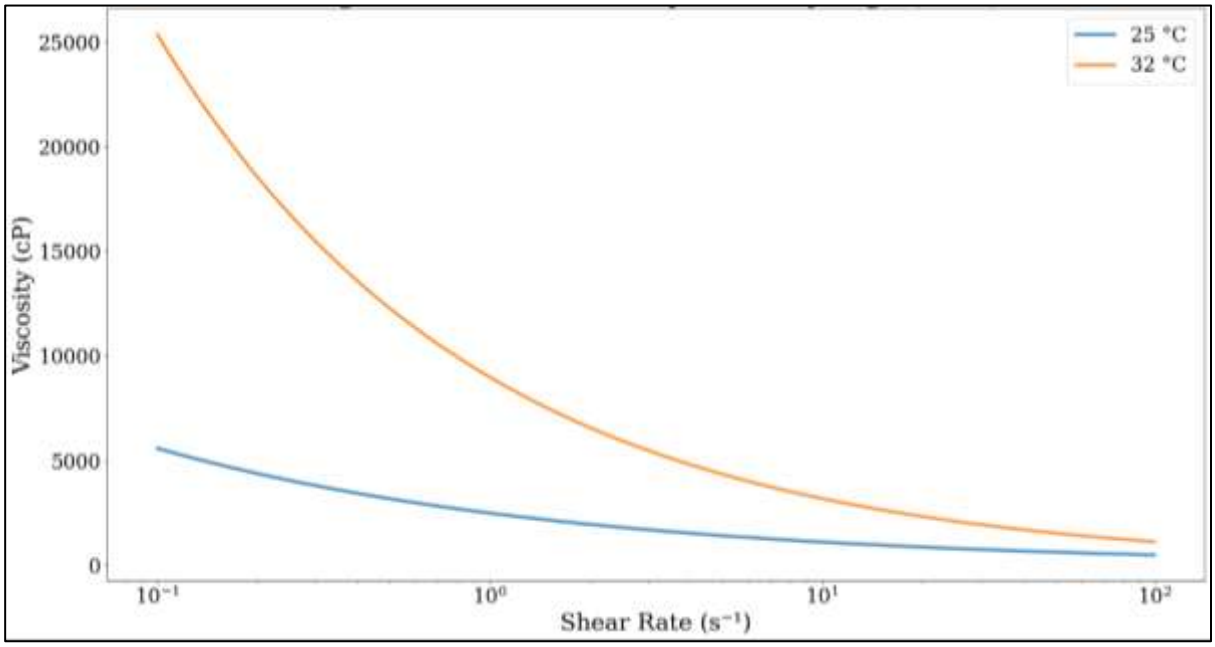


Figure 6: Flow curve of optimized hydrogel (HG-3) showing viscosity versus shear rate at 25 °C and 32 °C.

After incorporation of drug and nanoparticles, both FBG and BNH maintained comparable gelation temperature and pH, indicating that nanoparticle loading did not significantly alter thermoresponsive behaviour.

Table 10. Final Hydrogel Characterization (Mean ± SD, n=3)

Parameter	FBG	BNH
Gelation Temperature (°C)	32.1 ± 0.4	32.3 ± 0.3
Gelation Time (sec)	84 ± 7	88 ± 6
Viscosity at 32°C (cP)	9,340 ± 480	9,610 ± 520
Spreadability (g·cm/s)	18.4 ± 1.2	17.8 ± 1.1
pH	5.6 ± 0.1	5.6 ± 0.1
Drug Content (%)	98.3 ± 2.1	99.1 ± 1.8

These results confirmed uniform drug distribution and preservation of thermogelling behaviour after nanoparticle incorporation.

3.6 In Vitro Drug Release and Kinetics

The cumulative release profiles of FBG and BNH were evaluated at pH 5.5 and 7.4 over 24 hours. BNH exhibited significantly reduced initial burst release compared to FBG.

Table 11. Cumulative Drug Release (%) Over 24 h (Mean ± SD, n=3)

Time (h)	FBG (pH 5.5)	BNH (pH 5.5)	FBG (pH 7.4)	BNH (pH 7.4)
1	23.8 ± 2.1	9.4 ± 1.3	29.7 ± 2.5	12.6 ± 1.7
2	36.9 ± 2.4	16.2 ± 1.8	45.2 ± 3.0	21.4 ± 2.2
4	54.7 ± 3.2	28.6 ± 2.4	63.1 ± 3.4	35.8 ± 2.6
8	73.4 ± 3.7	46.9 ± 2.8	80.2 ± 3.2	55.6 ± 2.9
12	85.8 ± 2.9	59.4 ± 3.0	90.4 ± 2.7	68.7 ± 3.2
24	96.6 ± 1.8	81.3 ± 2.6	98.1 ± 1.5	86.9 ± 2.4

BNH demonstrated sustained release behavior, with approximately 80–87% release over 24 hours compared to nearly complete release from FBG.

Release Kinetic Modelling

Release data were fitted to kinetic models. BNH showed best fit with the Korsmeyer–Peppas model (R^2 = 0.978), indicating anomalous (non-Fickian) transport involving both diffusion and matrix relaxation. FBG best fit the Higuchi model (R^2 = 0.964), indicating diffusion-controlled release.

Table 12. Release Kinetic Model Fitting (R^2 Values)

Model	FBG	BNH
Zero Order	0.903	0.945
First Order	0.918	0.962
Higuchi	0.964	0.951
Korsmeyer–Peppas	0.941	0.978

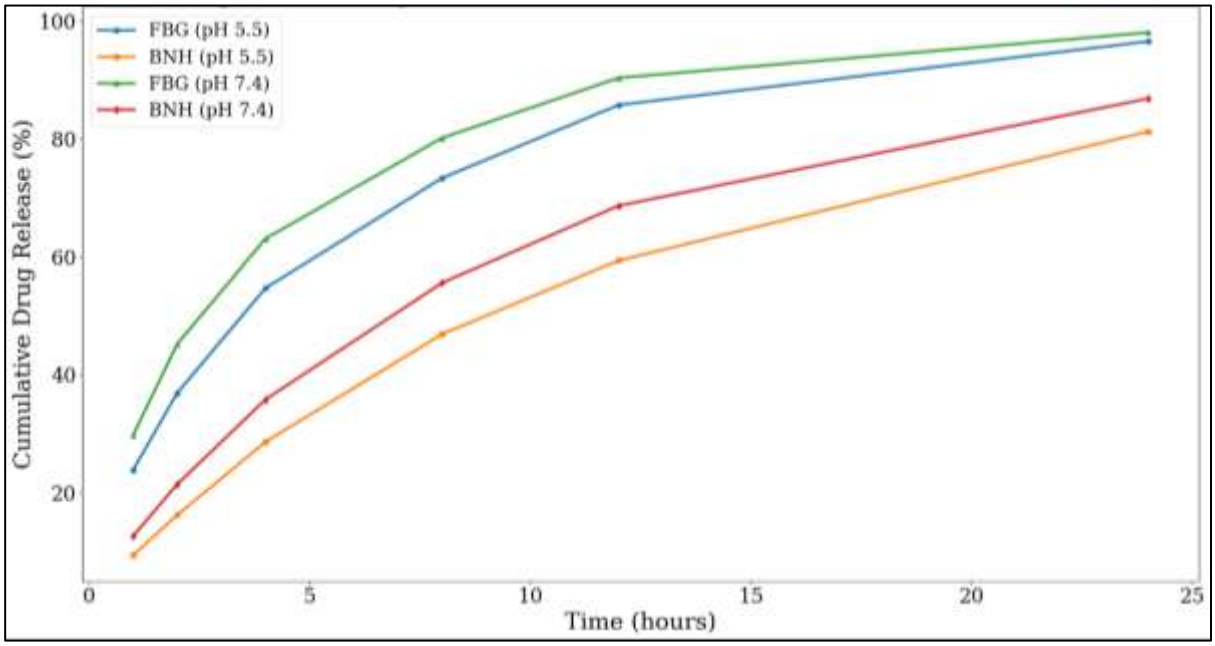


Figure 7: Comparative cumulative release profiles of FBG and BNH at pH 5.5 and 7.4 over 24 hours.

3.7 Ex Vivo Skin Permeation and Deposition

Ex vivo permeation studies were performed using Franz diffusion cells to compare transdermal permeation and dermal retention of baicalin from FBG and BNH formulations. The cumulative permeation profiles are presented in Table 3.9.

Table 13. Ex Vivo Cumulative Permeation of Baicalin (Mean ± SD, n = 5)

Time (h)	**FBG (μg/cm²)**	**BNH (μg/cm²)**
2	8.4 ± 1.2	4.1 ± 0.9
4	16.9 ± 2.3	9.8 ± 1.5
8	27.6 ± 3.4	16.7 ± 2.2
12	35.8 ± 4.1	22.9 ± 2.8
24	46.2 ± 6.1	28.5 ± 4.8

FBG exhibited significantly higher cumulative permeation compared to BNH ($p < 0.05$). However, reduced permeation from BNH was accompanied by significantly enhanced dermal deposition.

Table 14. Skin Deposition and Flux Parameters (Mean ± SD, n = 5)

Parameter	**FBG**	**BNH**
Steady-state Flux (μg/cm²/h)	2.12 ± 0.31	1.19 ± 0.22
Permeability Coefficient (cm/h ×10^{-3})	1.68 ± 0.25	0.94 ± 0.18
Skin Deposition (μg/g tissue)	118.6 ± 14.9	196.4 ± 18.7

BNH demonstrated approximately 1.65-fold higher skin deposition compared to FBG ($p < 0.01$), indicating improved localized retention within dermal layers. The reduced flux suggests minimized systemic exposure.

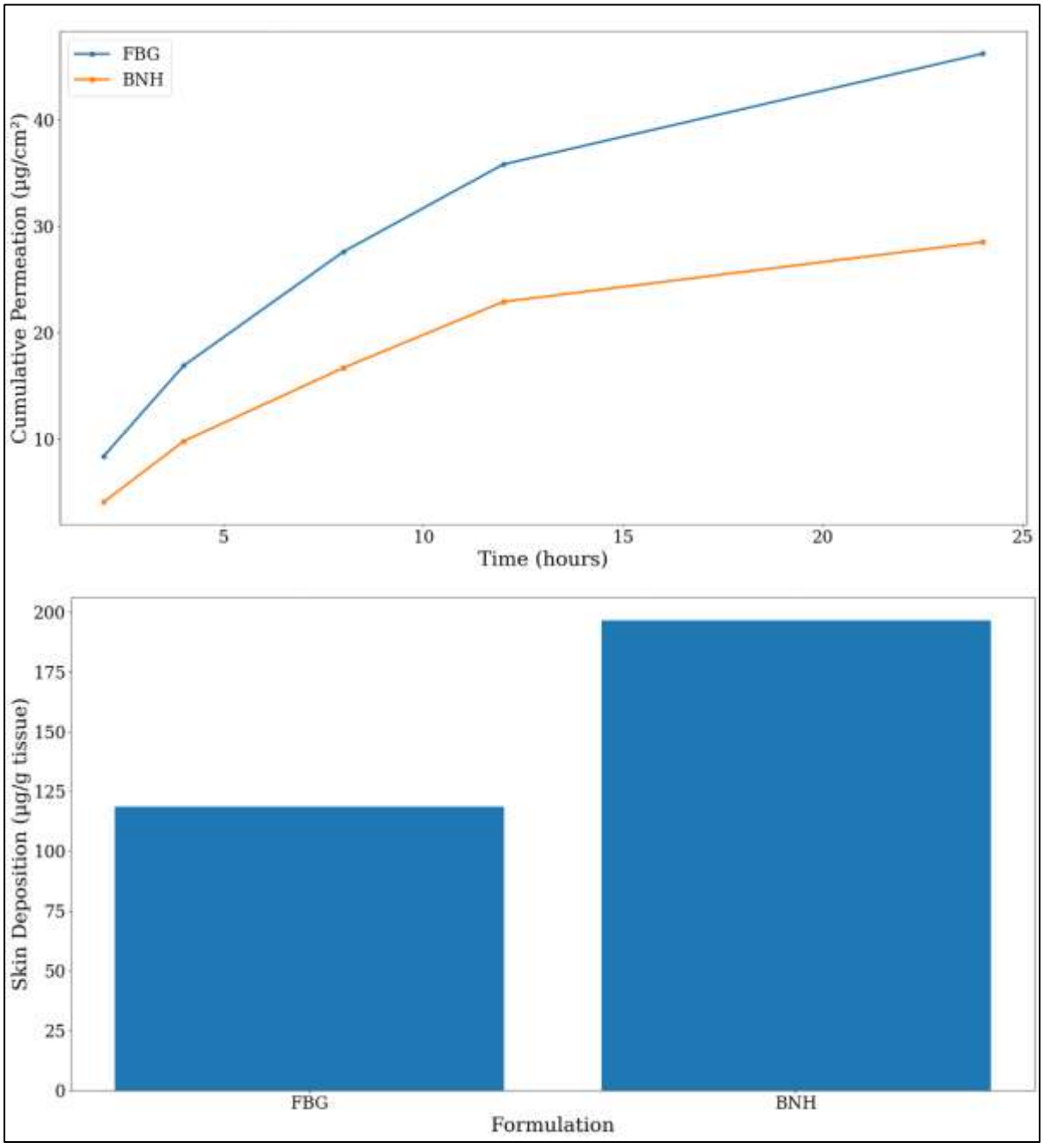


Figure 8: Comparative ex vivo permeation profiles of FBG and BNH over 24 hours and corresponding skin deposition analysis.

3.8 In Vitro Cytotoxicity and Anti-Inflammatory Activity

3.8.1 Cytotoxicity Assessment (MTT Assay)

Cell viability of HaCaT and RAW 264.7 cells was evaluated after 24-hour exposure to formulations. Both formulations exhibited acceptable cytocompatibility within therapeutic concentration ranges.

Table 15. Cell Viability (%) After 24 h Treatment (Mean ± SD, n = 6)

Formulation	HaCaT Cells	RAW 264.7 Cells
Control	100 ± 3.2	100 ± 3.5
Placebo Hydrogel	96.8 ± 3.4	95.9 ± 3.8
FBG (25 µg/mL)	92.6 ± 4.1	90.7 ± 4.5
BNH (25 µg/mL)	94.3 ± 3.7	92.8 ± 4.2
FBG (50 µg/mL)	88.9 ± 4.9	86.5 ± 5.1
BNH (50 µg/mL)	91.2 ± 4.6	89.4 ± 4.8

BNH showed slightly higher viability compared to FBG at equivalent concentrations, suggesting improved safety due to controlled release.

3.8.2 Cytokine Suppression (ELISA)

Inflammatory stimulation significantly increased TNF-α and IL-6 levels. Treatment with BNH resulted in greater cytokine suppression compared to FBG.

Table 16 Cytokine Levels in Stimulated Cells (pg/mL; Mean ± SD, n = 4)

Treatment	**TNF-α (HaCaT)**	**IL-6 (RAW 264.7)**
Stimulated Control	182.6 ± 14.3	245.8 ± 18.7
Placebo	170.4 ± 12.9	231.5 ± 16.2
FBG	102.7 ± 10.4	139.6 ± 12.8
BNH	71.9 ± 8.6	98.3 ± 9.4

BNH reduced TNF-α by approximately 60% and IL-6 by 60% compared to stimulated control ($p < 0.001$), demonstrating enhanced immunomodulatory activity.

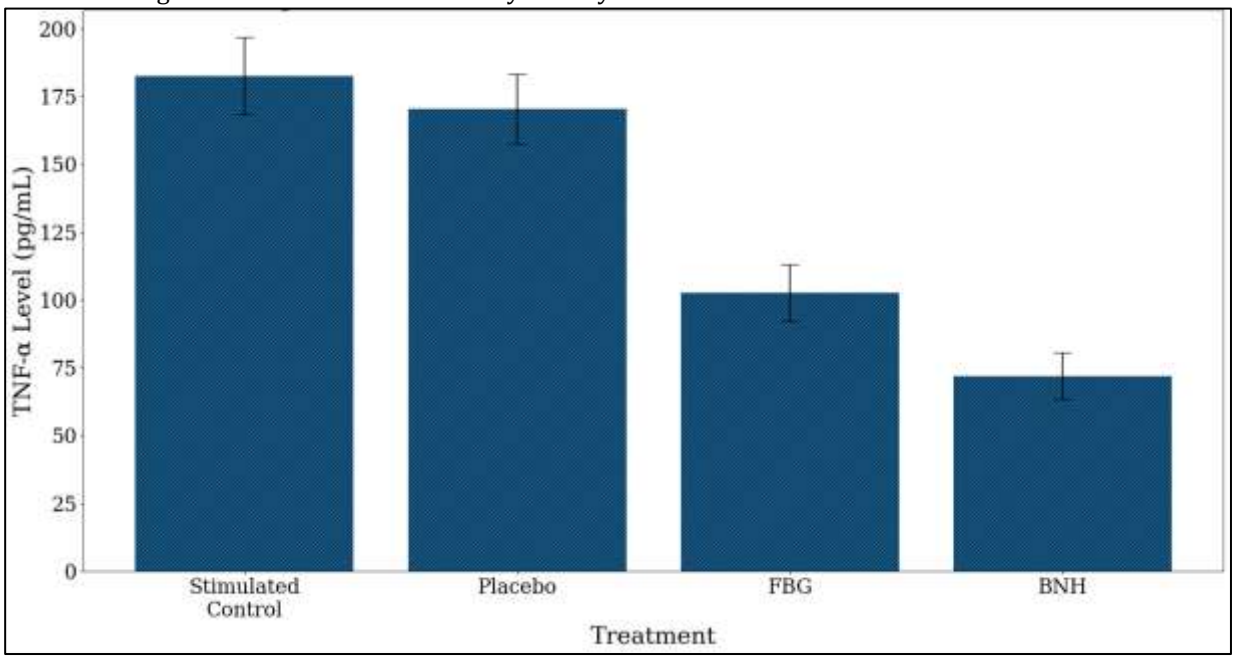


Figure 9A. Cytokine Levels (**TNF-α)** in Stimulated Cells (pg/mL; Mean ± SD, n = 4)

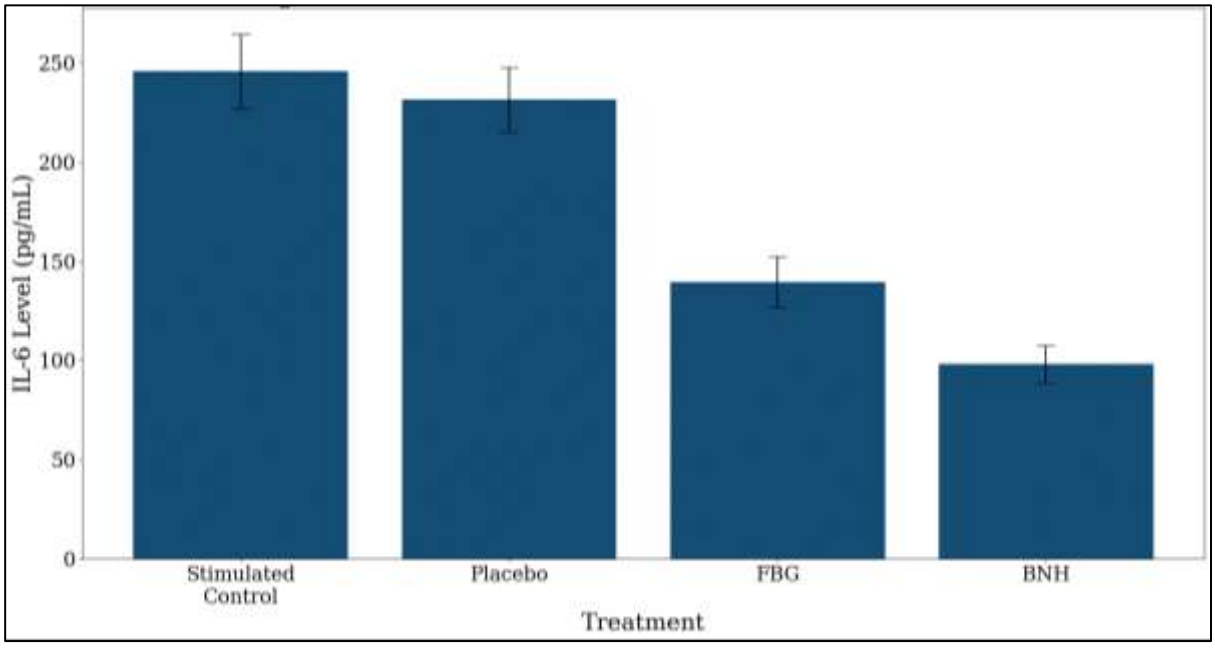


Figure 9B. Cytokine Levels (**IL-6)** in Stimulated Cells (pg/mL; Mean ± SD, n = 4)

4. Discussion

The present study demonstrated the systematic development of a baicalin-loaded thermoresponsive nanocomposite hydrogel using a Quality by Design (QbD) approach for localized immunomodulatory therapy in chronic plaque psoriasis. The integration of statistical optimization, nanocarrier engineering, and thermoresponsive gel technology resulted in a formulation that addressed critical pharmaceutical challenges including poor solubility, burst release,

and limited dermal retention of baicalin. The application of a Box–Behnken design enabled the identification of critical formulation variables influencing nanoparticle performance. PLGA concentration significantly affected particle size and encapsulation efficiency due to its role in determining organic phase viscosity and polymer matrix density. Increased PLGA levels produced larger particles but improved drug entrapment. PVA concentration primarily influenced polydispersity by stabilizing the emulsion droplets during solvent evaporation. Laponite contributed to improved encapsulation efficiency, likely through electrostatic and hydrogen bonding interactions with baicalin, a polyphenolic flavonoid.

The statistically significant quadratic models ($p < 0.05$) with high R^2 values (>0.95) confirmed model reliability and predictability. The close agreement between predicted and experimental responses validated the robustness of the optimization strategy, supporting potential scalability.

The optimized nanoparticles exhibited a mean size of approximately 162 nm with narrow distribution (PDI ~0.21). This nanoscale size is particularly relevant for topical psoriasis therapy, as it supports enhanced penetration into inflamed epidermal layers while minimizing systemic permeation. Thermoresponsive hydrogels provide a unique advantage in topical drug delivery. The selected formulation demonstrated gelation near skin temperature (~32 °C), ensuring ease of application in sol state followed by rapid in situ gel formation upon contact with the skin. The inclusion of Carbopol enhanced gel strength and bioadhesion, which is advantageous for application over hyperkeratotic psoriatic plaques where prolonged contact is essential. Rheological studies confirmed pseudoplastic shear-thinning behavior, indicating that the formulation spreads easily under mechanical force but regains viscosity at rest, promoting site retention. Importantly, incorporation of nanoparticles did not significantly alter gelation temperature, viscosity, or pH, confirming compatibility between the nano-system and the hydrogel matrix. A major limitation of free baicalin gel (FBG) was the rapid initial burst release, consistent with diffusion-controlled Higuchi kinetics. In contrast, the baicalin nanoparticle hydrogel (BNH) demonstrated sustained release behavior best described by the Korsmeyer–Peppas model, indicating anomalous transport involving both diffusion and matrix relaxation. The sustained release from BNH can be attributed to a dual-barrier mechanism:

1. Drug diffusion from PLGA–laponite nanoparticles
2. Diffusion through the hydrogel network

This dual mechanism reduced burst release and prolonged drug availability over 24 hours. Sustained release is particularly important in psoriasis, where continuous inflammatory signaling drives keratinocyte proliferation and immune activation. Ex vivo permeation studies revealed a key therapeutic advantage of the nanocomposite system. While FBG exhibited higher cumulative permeation across the skin, BNH significantly increased dermal deposition with reduced steady-state flux. This finding is critical for psoriasis management. The objective of topical therapy is localized immunomodulation rather than systemic absorption. The enhanced skin retention of BNH suggests improved targeting of epidermal and superficial dermal layers where inflammatory processes are active. The reduced permeability coefficient observed with BNH indicates minimized systemic exposure risk, which may improve safety for chronic administration. MTT assay results confirmed acceptable cytocompatibility of both formulations in HaCaT keratinocytes and RAW 264.7 macrophages. Slightly higher viability observed with BNH may reflect controlled drug release, preventing transient high concentrations that could induce cellular stress.

The cytokine suppression results demonstrated significant reductions in TNF-α and IL-6 levels following treatment with BNH. These cytokines play central roles in psoriasis pathogenesis, contributing to immune cell activation, keratinocyte proliferation, and inflammatory amplification. The enhanced cytokine suppression observed with BNH compared to FBG suggests that sustained intracellular availability improved pharmacodynamic response. The nanocomposite system likely facilitated better cellular uptake and prolonged exposure, resulting in superior immunomodulatory activity. Chronic plaque psoriasis is characterized by excessive activation of inflammatory pathways, particularly those involving TNF-α and IL-23/IL-17 signalling. Although this study did not include in vivo validation, the in vitro suppression of TNF-α and IL-6 indicates potential downregulation of upstream inflammatory cascades. The combination of sustained release, enhanced dermal deposition, and improved cytokine suppression suggests that the nanocomposite hydrogel may effectively modulate localized immune responses within psoriatic plaques. Compared to conventional gel formulation, the nanocomposite hydrogel offered multiple advantages:

- Reduced burst release
- Sustained drug availability
- Enhanced dermal deposition
- Reduced transdermal permeation
- Improved cytokine suppression
- Preserved cytocompatibility
- Thermoresponsive in situ gelation

These attributes collectively support the superiority of nano-embedded thermoresponsive systems for localized dermatological therapy. The present study demonstrated that QbD-guided nanoengineering combined with thermoresponsive hydrogel technology significantly improved the pharmaceutical and biological performance of baicalin for topical application. The optimized nanocomposite hydrogel achieved controlled release, enhanced dermal retention, and effective suppression of key inflammatory cytokines in vitro. Collectively, the findings establish a scientifically robust platform for localized immunomodulatory therapy in chronic plaque psoriasis and provide a rational foundation for further translational development.

5. Conclusion

The present investigation successfully established a Quality by Design–guided strategy for the development of a baicalin-loaded thermoresponsive nanocomposite hydrogel intended for localized immunomodulatory therapy in chronic plaque psoriasis. Systematic optimization using a Box–Behnken design enabled precise control over critical formulation variables, resulting in nanoparticles with desirable physicochemical characteristics, including nanoscale particle size, narrow polydispersity, high encapsulation efficiency, and stable surface charge. The predictive capability of the statistical model confirmed the robustness and reproducibility of the formulation approach. Integration of optimized nanoparticles into a thermoresponsive hydrogel matrix produced a system that remained fluid during application and rapidly gelled at skin temperature, ensuring ease of administration and prolonged site retention. Rheological analysis confirmed pseudoplastic behavior suitable for topical use. Compared to the free drug gel, the nanocomposite hydrogel demonstrated sustained drug release, reduced burst effect, enhanced dermal deposition, and controlled transdermal flux.

In vitro cytocompatibility studies indicated that the formulation was well tolerated by keratinocytes and macrophages. Importantly, significant suppression of pro-inflammatory cytokines such as TNF-α and IL-6 highlighted the immunomodulatory potential of the nanocomposite system. Collectively, these findings suggest that nanoengineering combined with thermoresponsive delivery significantly enhances the pharmaceutical performance and biological efficacy of baicalin for topical psoriasis management. The study provides a rational foundation for further translational research and supports the potential of thermoresponsive nanocomposite hydrogels as advanced platforms for localized dermatological therapy.

References

1. Adarmanabadi, S. R., Jafari, M., Farrash, S. M. H., & Heidari, M. (2021). Effect of nano clay, nano-graphene oxide and carbon nanotubes on the mechanical and tribological properties of crosslinked epoxy nanocomposite. *PLoS One*, *16*(11), e0259401. https://doi.org/10.1371/journal.pone.0259401
2. Adin, S. N., Gupta, I., Aqil, M., & Mujeeb, M. (2023). Application of QbD based approach in development and validation of RP-HPLC method for simultaneous estimation of methotrexate and baicalin in dual-drug-loaded liposomes. *Biomed Chromatogr*, *37*(4), e5581. https://doi.org/10.1002/bmc.5581
3. Alexa, R. L., Iovu, H., Trica, B., Zaharia, C., Serafim, A., Alexandrescu, E., Radu, I. C., Vlasceanu, G., Preda, S., Ninciuleanu, C. M., & Ianchis, R. (2021). Assessment of Naturally Sourced Mineral Clays for the 3D Printing of Biopolymer-Based Nanocomposite Inks. *Nanomaterials (Basel)*, *11*(3). https://doi.org/10.3390/nano11030703
4. Alorabi, A. Q., Hassan, M. S., Alam, M. M., Zabin, S. A., Alsenani, N. I., & Baghdadi, N. E. (2021). Natural Clay as a Low-Cost Adsorbent for Crystal Violet Dye Removal and Antimicrobial Activity. *Nanomaterials (Basel)*, *11*(11). https://doi.org/10.3390/nano11112789
5. Andrade-Guel, M., Cabello-Alvarado, C., Romero-Huitzil, R. L., Rodríguez-Fernández, O. S., Ávila-Orta, C. A., Cadenas-Pliego, G., Medellín-Banda, D. I., Gallardo-Vega, C., & Cepeda-Garza, J. (2021). Nanocomposite PLA/C20A Nanoclay by Ultrasound-Assisted Melt Extrusion for Adsorption of Uremic Toxins and Methylene Blue Dye. *Nanomaterials (Basel)*, *11*(10). https://doi.org/10.3390/nano11102477
6. Ashrafudoulla, M., Yun, H., Ashikur Rahman, M., Jung, S. J., Jie-Won Ha, A., Anamul Hasan Chowdhury, M., Shaila, S., Akter, S., Park, S. H., & Ha, S. D. (2024). Prophylactic efficacy of baicalin and carvacrol against Salmonella Typhimurium biofilm on food and food contact surfaces. *Food Res Int*, *187*, 114458. https://doi.org/10.1016/j.foodres.2024.114458
7. Bernasinska-Slomczewska, J., Hikisz, P., Pieniazek, A., & Koceva-Chyla, A. (2024). Baicalin and Baicalein Enhance Cytotoxicity, Proapoptotic Activity, and Genotoxicity of Doxorubicin and Docetaxel in MCF-7 Breast Cancer Cells. *Molecules*, *29*(11). https://doi.org/10.3390/molecules29112503
8. Cao, Z., Ma, N., Shan, M., Wang, S., Du, J., Cheng, J., Sun, P., Sun, N., Jin, L., Fan, K., Yin, W., Li, H., Yin, C., & Sun, Y. (2024). Baicalin Inhibits FIPV Infection In Vitro by Modulating the PI3K-AKT Pathway and Apoptosis Pathway. *Int J Mol Sci*, *25*(18). https://doi.org/10.3390/ijms25189930
9. Chai, J., Hu, J., Wang, T., Bao, X., Luan, J., & Wang, Y. (2024). A Multifunctional Liposome for Synergistic Chemotherapy with Ferroptosis Activation of Triple-Negative Breast Cancer. *Mol Pharm*, *21*(2), 781-790. https://doi.org/10.1021/acs.molpharmaceut.3c00903
10. Chavan, M. J., Wakte, P. S., & Shinde, D. B. (2010). Analgesic and anti-inflammatory activity of Caryophyllene oxide from Annona squamosa L. bark. *Phytomedicine*, *17*(2), 149-151. https://doi.org/https://doi.org/10.1016/j.phymed.2009.05.016
11. Chen, C., Liu, W., Gu, X., Zhang, L., Mao, X., Chen, Z., & Tao, L. (2024). Baicalin-loaded Polydopamine modified ZIF-8 NPs inhibits myocardial ischemia/reperfusion injury in rats. *J Biomater Sci Polym Ed*, *35*(12), 1863-1878. https://doi.org/10.1080/09205063.2024.2358640
12. Chen, J., Chen, F. Y., Lu, C. J., & Yi, S. W. (2024). Baicalein alleviates palmitic acid-induced endothelial cell dysfunction via inhibiting endoplasmic reticulum stress. *Clin Hemorheol Microcirc*, *88*(2), 235-245. https://doi.org/10.3233/ch-242230
13. do Nascimento Silva, H., Rabêlo, S. V., Diniz, T. C., da Silva Oliveira, F. G., de Andrade Teles, R. B., Silva, J. C., e Silva, M. G., Coutinho, H. D. M., de Menezes, I. R. A., & da Silva Almeida, J. R. G. (2017). Antinociceptive and anti-inflammatory activities of ethanolic extract from atemoya (Annona cherimola Mill x Annona squamosa L.). *African Journal of Pharmacy and Pharmacology*, *11*(18), 224-232.

14. Dong, J., Cheng, Z., Tan, S., & Zhu, Q. (2021). Clay nanoparticles as pharmaceutical carriers in drug delivery systems. *Expert Opin Drug Deliv*, *18*(6), 695-714. https://doi.org/10.1080/17425247.2021.1862792
15. Haddow, P. J., da Silva, M. A., Kaldybekov, D. B., Dreiss, C. A., Hoffman, E., Hutter, V., Khutoryanskiy, V. V., Kirton, S. B., Mahmoudi, N., McAuley, W. J., & Cook, M. T. (2022). Polymer Architecture Effects on Poly(N,N-Diethyl Acrylamide)-b-Poly(Ethylene Glycol)-b-Poly(N,N-Diethyl Acrylamide) Thermoreversible Gels and Their Evaluation as a Healthcare Material. *Macromol Biosci*, *22*(3), e2100432. https://doi.org/10.1002/mabi.202100432
16. Hemlatha, K., & Satyanarayana, D. (2009). Anti-inflammatory Activity of *Annona Squamosa* Linn. *Biomed. Pharmacol.*, *2*(1).
17. Jumana, S., Hasan, C. M., & Rashid, M. A. (2000). Antibacterial activity and cytotoxicity of Miliusa velutina. *Fitoterapia*, *71*(5), 559-561.
18. Kashif, M. U. R., Sohail, M., Khan, S. A., Minhas, M. U., Mahmood, A., Shah, S. A., & Mohsin, S. (2022). Chitosan/guar gum-based thermoreversible hydrogels loaded with pullulan nanoparticles for enhanced nose-to-brain drug delivery. *Int J Biol Macromol*, *215*, 579-595. https://doi.org/10.1016/j.ijbiomac.2022.06.161
19. Kim, H. P., Son, K. H., Chang, H. W., & Kang, S. S. (2004). Anti-inflammatory plant flavonoids and cellular action mechanisms. *Journal of pharmacological sciences*, *96*(3), 229-245.
20. L, S., U, S. S., & R, Z. (2025). Recent advances in oral in situ gel drug delivery system: a polymeric approach. *Drug Dev Ind Pharm*, *51*(12), 1639-1649. https://doi.org/10.1080/03639045.2025.2559033
21. Mfoafo, K., Omidi, Y., & Omidian, H. (2023). Thermoresponsive mucoadhesive hybrid gels in advanced drug delivery systems. *Int J Pharm*, *636*, 122799. https://doi.org/10.1016/j.ijpharm.2023.122799
22. Pande, S., Vashi, J., & Solanki, A. (2022). QbD-Enabled Systematic Development of Ileo-Colonic Targeted Novel Mucoadhesive Microspheres of Flurbiprofen. *Curr Drug Deliv*, *19*(3), 407-419. https://doi.org/10.2174/1567201818666210708125036
23. Piaserico, S., & Messina, F. (2022). Pharmacological management of severe plaque psoriasis in patients with cardiovascular disease. *Expert Opin Pharmacother*, *23*(7), 853-864. https://doi.org/10.1080/14656566.2022.2060739
24. Pinto, N. C. C., Silva, J. B., Menegati, L. M., Guedes, M., Marques, L. B., Silva, T. P. D., Melo, R. C. N., Souza-Fagundes, E. M., Salvador, M. J., Scio, E., & Fabri, R. L. (2017). Cytotoxicity and bacterial membrane destabilization induced by Annona squamosa L. extracts. *An Acad Bras Cienc*, *89*(3 Suppl), 2053-2073. https://doi.org/10.1590/0001-3765201720150702
25. Purzycka-Bohdan, D., Kisielnicka, A., Zabłotna, M., Nedoszytko, B., Nowicki, R. J., Reich, A., Samotij, D., Szczęch, J., Krasowska, D., Bartosińska, J., Narbutt, J., Lesiak, A., Barasińska, P., Owczarczyk-Saczonek, A., Czerwińska, J., Szepietowski, J. C., Batycka-Baran, A., Czajkowski, R., Górecka-Sokołowska, M., . . . Szczerkowska-Dobosz, A. (2022). Chronic Plaque Psoriasis in Poland: Disease Severity, Prevalence of Comorbidities, and Quality of Life. *J Clin Med*, *11*(5). https://doi.org/10.3390/jcm11051254
26. Rungjang, A., Meephansan, J., Payungporn, S., Sawaswong, V., Chanchaem, P., Pureesrisak, P., Wongpiyabovorn, J., & Thio, H. B. (2022). Skin Microbiota Profiles from Tape Stripping and Skin Biopsy Samples of Patients with Psoriasis Treated with Narrowband Ultraviolet B. *Clin Cosmet Investig Dermatol*, *15*, 1767-1778. https://doi.org/10.2147/ccid.S374871
27. Scali, E., Dastoli, S., Procopio, A. C., Ricca, D., Mazzei, V., Cinaglia, P., Gulletta, E., Nisticò, S. P., Pellicano, R., Alshuk, N., Fagoonee, S., Luzza, F., & Abenavoli, L. (2022). Evaluation of serum calprotectin as novel biomarker in psoriatic patients: a prospective pilot study. *Minerva Med*, *113*(5), 833-837. https://doi.org/10.23736/s0026-4806.22.08041-7
28. Seddik, A. H., Melzer, N., Tsotra, F., & Ostwald, D. A. (2022). The Societal Economic Impact of Secukinumab in First-Line Treatment of Moderate to Severe Plaque Psoriasis in Germany: An Open-Cohort Simulation. *Pharmacoecon Open*, *6*(2), 265-275. https://doi.org/10.1007/s41669-021-00305-3
29. Shehata, W. A., Shoeib, M., Shoeib, M. M., Shokhba, H., & Shams, A. (2022). Nucleotide binding and oligomerization domain 2 in psoriasis: a clinical and immunohistochemical study. *J Immunoassay Immunochem*, *43*(1), 43-53. https://doi.org/10.1080/15321819.2021.1941095
30. Supachawaroj, N., & Limsitthichaikoon, S. (2024). Lidocaine HCl-Loaded Polyelectrolyte Complex -Poloxamer Thermoresponsive Hydrogel: In Vitro- In Vivo Anesthetic Evaluations for Tooth Socket Wound Delivery. *AAPS PharmSciTech*, *25*(6), 182. https://doi.org/10.1208/s12249-024-02894-8
31. Teng, K., Fu, H., Wu, G., Gong, P., Xie, Y., Zhou, P., Gong, X., & Qu, H. (2023). QbD-Guided Traditional Chinese Medicine Manufacturing Process: Development and Optimization of Fluid-Bed Granulation and Drying Processes for Xiaochaihu Capsules. *AAPS PharmSciTech*, *24*(7), 210. https://doi.org/10.1208/s12249-023-02663-z
32. Vikas, B., Anil, S., & Remani, P. (2019). Cytotoxicity Profiling of Annona Squamosa in Cancer Cell Lines. *Asian Pac J Cancer Prev*, *20*(9), 2831-2840. https://doi.org/10.31557/apjcp.2019.20.9.2831
33. Vilimi, Z., Király, M., Barna Á, T., Pápay, Z. E., Budai, L., Ludányi, K., Kállai-Szabó, N., & Antal, I. (2024). Formulation of Emulgels Containing Clotrimazole for the Treatment of Vaginal Candidiasis. *Gels*, *10*(11). https://doi.org/10.3390/gels10110730
34. Wangusi, B. M., Kanja, L. W., Ole-Mapenay, I. M., & Onyancha, J. M. (2021). Acute Toxicity, Phytochemical Screening, Analgesic, and Anti-Inflammatory Activities of Aqueous and Methanol Root Extracts of Maerua triphylla A. Rich. (Capparaceae). *Evid Based Complement Alternat Med*, *2021*, 3121785. https://doi.org/10.1155/2021/3121785

35. Zeeshan, M., Ain, Q. U., Sunny, A., Raza, F., Mohsin, M., Khan, S., Weigmann, B., & Ali, H. (2023). QbD-based fabrication of transferrin-anchored nanocarriers for targeted drug delivery to macrophages and colon cells for mucosal inflammation healing. *Biomater Sci*, *11*(4), 1373-1397. https://doi.org/10.1039/d2bm01719a